Research Article

Nano Research
2019, 12(11): 2788–2795

ISSN 1998-0124 CN 11-5974/O4
https://doi.org/10.1007/s12274-019-2514-5

Large-scale highly ordered periodic Au nano-discs/graphene and graphene/Au nanoholes plasmonic substrates for surface-enhanced Raman scattering

Yansheng Liu and Feng Luo (✉)

IMDEA Nanoscience, Faraday 9, Ciudad Universitaria de Cantoblanco, Madrid 28049, Spain

Received: 19 July 2019 / **Revised:** 2 September 2019 **Accepted:** 3 September 2019

ABSTRACT

In this paper, the study of using masks to directly generate large area, highly ordered and periodical nanostructure has been exhibited. Periodic Au nano-discs(NDs) arrays have been fabricated on top of graphene by using holey Si_3N_4 mask which is directly fixed on top of graphene and Au metal is deposited through the holes in mask by thermal evaporation method under vacuum condition. This fabrication method provides an easy, fast and cost efficiency way to generate periodical nanostructure. Also, Au nanoholes(NHs) structure has been studied by using holey Si_3N_4 as a template. The surface-enhanced Raman scattering (SERS) sensitivities of periodical Au NDs/graphene and graphene/Au NHs hybrid structures have been systematically studied. The internal mechanisms could be explained by chemical mechanism effect of graphene and electromagnetic mechanism effect of metallic nano-structures. The enhancement factors have been systematically investigated by varying the diameter and the thickness of Au discs and Au NHs. Raman mappings of Au NDs with 2.5 μm diameter illustrate that the larger SERS enhancements exist in the rim of NDs which has good agreement with the electric field simulation result. The SERE enhancement factors of fluorescein obtained from Au NDs/graphene substrates shows an improvement factor of 500% in comparison of graphene substrate. The calculated SERS enhancement factors of graphene/Au NHs achieve 1,200% in comparison of graphene/planar Au film substrate.

KEYWORDS

graphene, surface-enhanced Raman scattering (SERS), Au nano-discs (NDs), Au nanoholes (NHs), periodic

1 Introduction

In the past decades, Raman spectroscopy has been regarded as a very important, promising and powerful technique in characterizing the structure of chemical materials without any damages [1]. In the beginning, Raman spectroscopy technology was neglected because of its weak intensity, inelastic scattering process with a very low cross-section, fluorescence interference, inefficient light collection and detection [2–6]. These defects have limited analysis efficiency and applicability of Raman scattering. Consequently, finding a way to enhance signals of Raman spectroscopy is a long-term pursuit, no matter in theory studying or in practical meaning. Surface-enhanced Raman scattering (SERS) provides an opportunity to make Raman as a powerful technique for ultrasensitive and selective detection in biology and chemistry. Currently, SERS is the only method capable of simultaneously detecting a single molecule and providing its chemical fingerprint [2, 7–10]. Normally, two widely accepted mechanisms are chemical mechanism (CM) and electromagnetic mechanism (EM) [2, 7]. The CM is mainly caused by charge transfer between target molecules and substrate, usually it has a minor enhancement factor of 10–100 [8]. The EM is based on local electromagnetic field caused by surface excitation plasmon under light illuminate condition. The enhancement of electromagnetic field results in a significant increase in the cross section of the Raman scattering and up to 10^8 or more [4, 11, 12].

The CM is usually thought to be a "first layer effect" because that the charge transfer needs less distance. Some studies show that the first monolayer molecules absorbed on substrate often exhibit a SERS cross section which is much larger than that of the second layer [11]. For such reason, a uniform and small roughness surface is needed to get much chemically enhanced signal. In comparison with other kinds of materials, monolayer graphene with homogenous and quite flat surface comes into our sight. As a two-dimension (2D) material, monolayer graphene is composed of carbon atoms with a hexagonal lattice structure. It has lots of interesting properties such as atomic thickness, high thermal conductivity [12], high current density [13], intrinsic field-effect mobility [14], and transparency (2.3% light absorption at normal incidence)[15]. In addition, graphene possesses characters of excellent bio-compatibility and chemical stability. So, considerable efforts have been devoted to graphene SERS sensors in identification and detection of chemical and biological species in a label-free environment [16, 17]. For EM effect, metallic plasmonic nanostructures are regarded as the most promising candidates for applications in SERS [8]. The metallic nanostructures possess very important properties, one of which is the possibility of a collective excitation of conduction electrons by UV-visible light. This excitation, known as surface plasmon excitation, is responsible for remarkable size/shape/environment-dependent optical properties of metallic nanostructures [18]. Plasmon excitation leads to strongly enhanced electromagnetic fields near the nanoparticle surfaces, and this is responsible for the electromagnetic contribution to the Raman signals observed in SERS [2, 11]. As a result, molecules adsorbed near the

Address correspondence to feng.luo@imdea.org

electromagnetic hot spots dominate the Raman intensity. Various metallic nanostructures with tuneable plasmonic properties have been widely explored as excellent SERS active systems [19, 20]. In the work of Cheng Mu, Au nano-particles (NPs) were spin-coated on prepared substrate with small channel to align Au NPs [21]. Au NPs modified substrate was fabricated through directly immersing the organic group pre-modified substrate into colloid suspension [22]. Isolated Au nanoparticles substrate was generated using O_2 plasma treat Au film [23]. In addition, periodical structures have been studied, such as using AAO template to get Au pillars [24], focus ion beam to fabricate Au nanorod [25, 26] and electron beam lithography (EBL) to generate Au disc [2]. The advances in colloidal synthesis methods and nanofabrication techniques such as e-beam and nanosphere lithography now allow for the fabrication of well-defined nanoparticles and therefore more homogeneous structures [16–18], but these methods need advanced instruments, several fabrication steps and longer time. So, finding an easy approach way to fabricate large area, highly ordered and periodical nanostructure is still an interesting topic. In this study, we provide a simple and efficient approach to achieve a hybrid system by sandwiching a monolayer graphene between periodic Au nanostructures and SiO_2/Si substrate. Graphene is transferred on SiO_2/Si and Au atoms go through the holes in Si_3N_4 mask to form Au NDs. Designing such structure combined EM and CM is a promising strategy in SERS performance. Thus, this combination of graphene and metallic plasmonic nanostructures is an effective way to enhance light matter interaction within visible wavelengths, which also could encourage potential applications in other fields. The role of graphene played in this structure graphene is an atomically thin, seamless, and chemically inert net with few functions which are: 1) ultrathin graphene layer can provide effective transfer of the electromagnetic field from the metallic structure through to the probe molecule; 2) graphene can efficiently reduce the fluorescence background of dye molecules which make the Raman scattering signal much clear; 3) the charge transfer between monolayer graphene and probe molecules is much easier. By varying diameter and thickness of the Au NDs and Au NHs, SERS enhancement factor has a good agreement with the electromagnetic field simulation results of NDs and NHs.

2 Experimental

2.1 Materials

Fluorescein molecules powder is purchased from Sigma-Aldrich. The holey Si_3N_4 masks and Kapton® tape are purchased from TED PELLA, INC. The gold wire with a diameter of 0.25 mm and purity of 99.99% is ordered from ADVENT Research Materials Ltd.

2.2 Characterization and instruments

Scanning electron microscope (SEM, JSM-6700F) and atomic force microscope (AFM, NT-MAT) were used to characterize the morphology of Au NPs deposited on substrates, before and after graphene transfer. Bruker OPUS Raman system was applied in SERS measurement.

2.3 Details of transferring graphene from copper foil to SiO_2/Si substrate

Graphene was synthesized by atmospheric pressure chemical vapor deposition (CVD) at 1,000 °C on copper foil with methane as carbon source [27]. In order to get a clean substrate surface, SiO_2/Si substrate was immersed into acetone ultrasound bath and ethanol ultrasound bath alternately for several times. After the cleaning process, nitrogen gas was applied to dry the substrate. Graphene grown on copper foil was cut into 4 cm × 4 cm square and then fixed onto one piece of clean normal glass by using Kapton® tape. Commercially available PMMA solution (A4 solution) had been spin coated on the top of graphene surface in order to generate support film at a speed of 4,000 r/min for 1 min. Remove the tape and turn the PMMA/graphene/copper sample upside down and then fixed it on one piece of clean glass, it should be noticed that the PMMA film now was facing the glass. Treat the sample with O_2 plasma for 2 min under condition of 150 mL/min O_2 flow speed, 100 W supplied power. The purpose of this treatment was aiming to remove the backside graphene. Cut PMMA/graphene/copper sample in a certain size and then put on APS solution (0.1 g/mL) for 2 h in order to etch copper foil. After Cu was completed etched, a clean process was necessary for transferring PMMA/graphene sample onto a water bath three times and the total cleaning time was 30 min. After that transfer PMMA/graphene on SiO_2/Si substrate and keep PMMA/graphene/SiO_2/Si sample into desiccator for 24 h under vacuum. After that acetone bath was applied to remove PMMA supporting film for several times. At last use N_2 gas to dry the graphene surface.

2.4 Fabrication and characterization of the Au array on graphene

The fabrication procedure of the highly periodic Au NDs on SiO_2/Si and graphene/SiO_2/Si substrates is schematically illustrated in Fig. 1. Si_3N_4 membrane with 200 nm thickness was directly fixed on top of SiO_2/Si or graphene/SiO_2/Si substrates surface by Kapton® tape. Then the sample was transferred into thermal evaporation chamber overnight under a pressure of 8.6×10^{-8} mbar in order to get better contact between Si_3N_4 membrane and the sample surface. The Au depositing process was under the pressure of 2×10^{-7} mbar. The thermal evaporation rate was at 20–30 Å/s. The Au NDs' thickness was monitored by a quartz balance and the final diameter and thickness were confirmed by AFM measurement.

2.5 SERS experiments

SERS experiments were carried out using a Raman system (OPUS) with laser excitation at 532 nm. The excitation laser spot was about 1 μm and the effective power of the laser source was kept at 2 mW for fluorescein molecules. The system is connected to a microscope, and the laser light was coupled through an objective lens of 50×, which was used for exciting the samples as well as collecting the Raman signals. Prior to each Raman experiment, calibration of the instrument was done with the Raman signal from a silicon standard centered at 520 cm^{-1}. SERS substrates were spin coated fluorescein solution at a speed of 4,000 r/min for 1 min. The SERS measurements

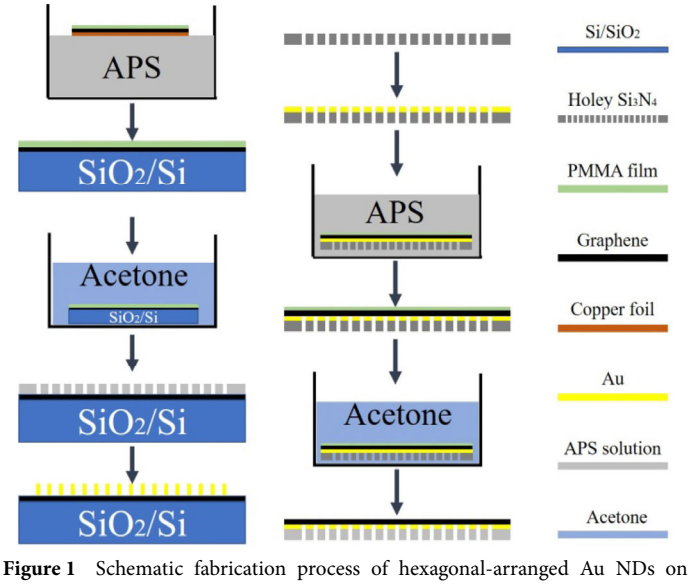

Figure 1 Schematic fabrication process of hexagonal-arranged Au NDs on graphene using holey Si_3N_4 mask and fabrication of graphene/Au NHs structure.

were performed from at 8 random locations in the NDs area and another 8 random locations which are located out of Au NDs but on the graphene with an accumulation time of 1 s. If there was no special instruction, the mentioned Raman spectra were expressed in terms of average spectra.

3 Results and discussion

The fabrications of periodical Au NDs/graphene (left side) and graphene/Au NHs structures (right side) are illustrated in Fig. 1. Firstly, PMMA/graphene/copper was put in APS solution in order to remove copper. Then acetone was applied to remove PMMA thin film which served as a support film. After that the Si_3N_4 mask was directly fixed on the top of graphene and then using thermal evaporation method to generate Au NDs. For graphene/Au nanohole structure, the Au film was directly evaporated on the top of holey Si_3N_4 and then graphene was transferred on the top. The fabrication details had been described in experimental section.

3.1 Characterization of Au NDs arrays

Figure 2 shows the SEM images of hexagonally arranged Au NDs deposited on SiO_2/Si substrate and graphene/SiO_2/Si substrate which was used Si_3N_4 membrane as mask. The diameter of both discs is 1 μm and the edge to edge distance is nearly 200 nm. In comparison with Au disc on SiO_2/Si substrate and graphene, the edge of Au disc on SiO_2/Si substrate is much sharper. This phenomenon is caused by the un-flat surface of graphene. The possibility of generated wrinkle, breaking area and PMMA residue in transferring process of graphene result in a larger gap between the mask and graphene surface which caused the diffusion of Au atoms.

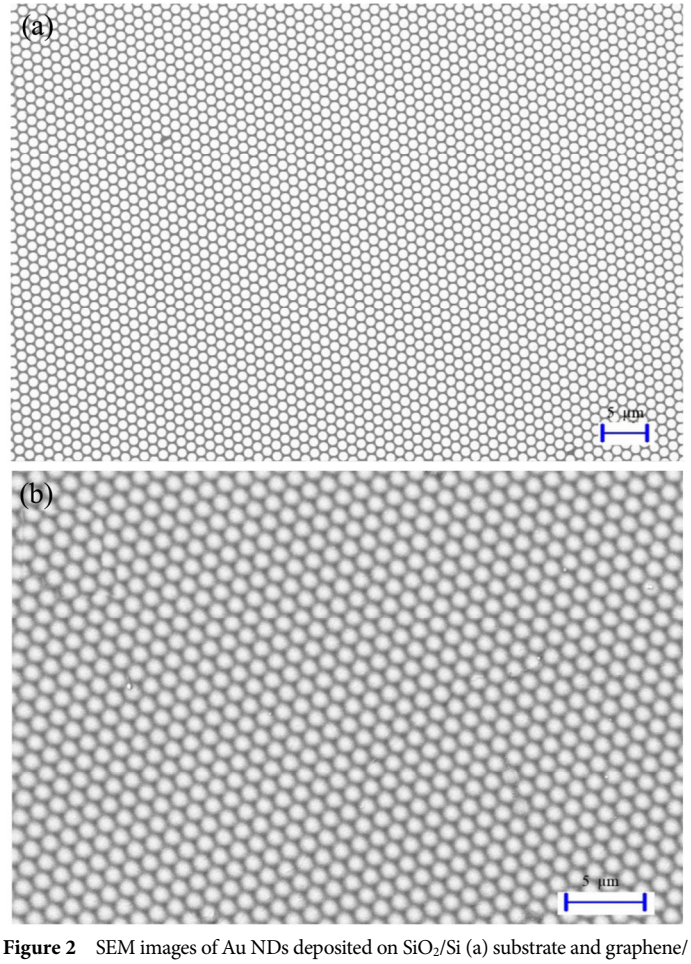

Figure 2 SEM images of Au NDs deposited on SiO_2/Si (a) substrate and graphene/SiO_2/Si (b) substrates. Blurred structures appearing in (b) indicate diffusion of Au atoms during deposition.

Figures 3(a) and 3(d) are AFM images of periodic Au NDs grown on graphene substrate with different thicknesses and diameters. After evaporation and peeling the Si_3N_4 mask off, the periodic and uniform Au NDs array grown on the graphene surface with hexagonal structure can be clearly observed which indicated the successful fabrication. The diameter of NDs is controlled by using different masks with certain nanoholes diameters and the thickness of NDs is controlled by evaporation time. Through the line cross-sections profiles, the diameter and the thickness of NDs in Figs. 3(a)–3(d) can be easily calculated and the corresponding diameter and thickness are 500 nm and 10 nm, 500 nm and 20 nm, 1 μm and 10 nm, 1 μm and 20 nm, respectively. The Au NDs on graphene surface are regarded as electromagnetic "hot spots" under light illumination, which can make the final combined structure exhibit electromagnetic enhancement active. Figures 3(e)–3(g) are AFM images of graphene/Au NHs substrates and the thickness of Au is 40 nm which calculated through the film thickness balance during evaporation process. The diameter of Au NHs in Figs. 3(e)–3(g) are 1,000, 500, and 300 nm respectively. From Figs. 3(e)–3(g), it can be clearly seen that the graphene film has been successfully transferred on the Au NHs. In addition, the broken area of graphene film also could be observed which look like "black holes" with big contrast.

3.2 SERS activities of Au NDs/graphene and graphene/Au NHs substrates

In order to detect the SERS property of different substrates, fluorescein has been used as a probe molecule. In this experiment fluorescein ethanol solution (1×10^{-3} mol/L) is spin coated on clean SiO_2/Si substrate, graphene/SiO_2/Si substrate, planar Au film, graphene/planar Au film and Au NDs/graphene substrate and graphene/Au NHs. In SERS experiment, samples with spin coated molecules are put on a high-speed encoded stage which has been controlled by the build-in Raman system software. In such case the sample can be automatically moved in XYZ directions by simply marking the area or points.

Figures 4(a) and 4(b) are obtained Raman spectra of different substrates. As shown in Fig. 4(a), Raman spectrum of fluorescein molecule spin coated on SiO_2/Si and planar Au film is quite weak and very noisy and the Raman signal of fluorescein spin coated on planar Au film also is very weak. In comparison with SiO_2/Si substrate, planar Au film substrate does not show any enhancement. This is expectable because that the planar Au film does not have any plasmonic effect. For the graphene/SiO_2/Si substrate and graphene/planar Au film substrate, peaks located at 595, 636, 763, 1,182, 1,331, 1,409, 1,549 and 1,634 cm^{-1} can be clearly observed. The Raman frequency range from 1,000 to 1,800 cm^{-1} contains skeletal vibrational modes of the xanthene moiety of fluorescein [28–30] and the torsional motions between the xanthene ring and benzoate are below 1,000 cm^{-1}. These peaks are in good agreement with previous reports for Raman shift of fluorescein molecules [28]. By comparison, the signal of molecules on the graphene sample is much stronger than the sample without graphene. This result indicates the chemical enhancement of graphene. Graphene as a two-dimensional material provides a surface with more well-defined molecule–substrate interactions such as molecules absorption and charge transfer between molecule and graphene [31]. In comparison with Raman signals intensities of fluorescein molecules on graphene/planar Au substrate, the signal graphene substrate intensity does not show much difference. This result demonstrates that the planar Au film does not show any interactions with graphene and does not contribute to the enhancement of Raman signal. The Raman signal of fluorescein molecules which located on periodical Au array and Au array/graphene substrate exhibits an excellent enhancement, due to localized surface plasmon resonance (LSPR) of highly uniform Au NDs arrays. The average enhancement of Au array/graphene is

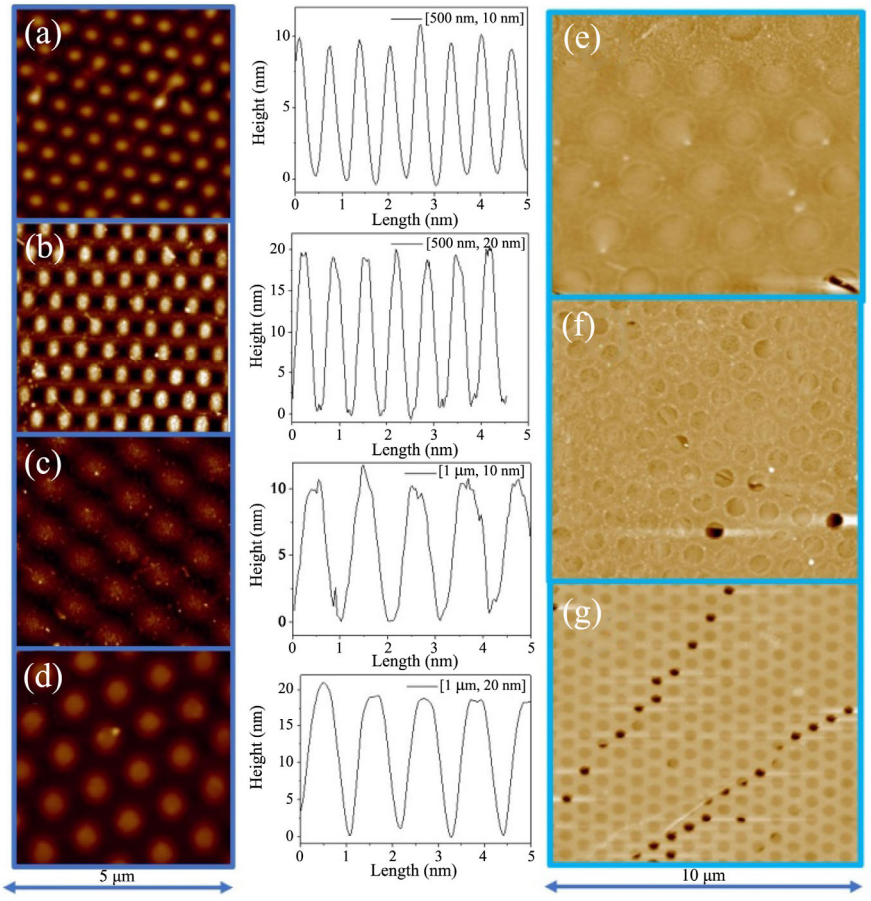

Figure 3 (a)–(d) AFM images (5 μm × 5 μm) of Au NDs deposited on graphene/SiO_2/Si substrate with different diameters and thicknesses. The cross-section profiles illustrate the thickness and the diameter of corresponding Au NDs. The corresponding diameter and thickness in (a) and (d) are 500 and 10 nm, 500 and 20 nm, 1 μm and 10 nm, 1 μm and 20 nm, respectively. (e)–(g) AFM images (10 μm × 10 μm) of transferred graphene on Au NHs with different diameter under the Au thickness of 40 nm. The diameters of Au hole are 1 μm (e), 500 nm (f) and 300 nm(g).

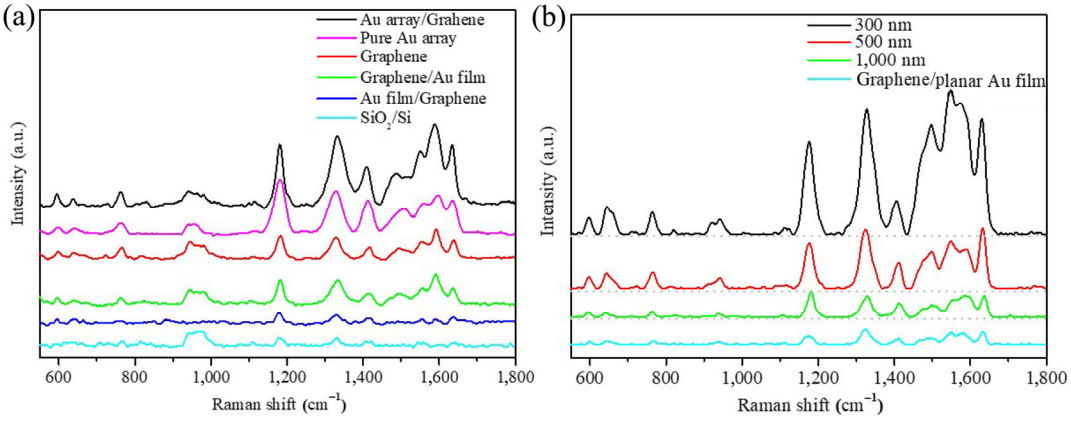

Figure 4 (a) Raman spectra of fluorescein spin coated on SiO_2/Si and SERS spectra fluorescein which spin coated on Au film, pure Au NDs substrate, graphene, graphene/Au film and Au NDs/graphene. (b) Raman spectra of fluorescein spin coated on graphene/Au NHs with different diameters.

larger than pure Au array substrate due to the CM enhancement of graphene between NDs. The highly uniform Au NDs arrays fabricated on certain substrates over large surfaces are efficient "hot spots" which make the final combined structure exhibits electromagnetic enhancement active resulting in enhancing the Raman signals of molecules. For such reason, generated the electric field of Au NDs dramatically enhancement the vibration of the molecules. After calculating the enhancement of Au NDs/graphene sample, the enhancement is 5 times larger than fluorescein on the graphene substrate. For the Au NHs samples, rim of Au NHs contributes to the magnetoelectrical field which results in the enhancement. Obtained Raman spectrum of Au NHs samples are similar to Au NDs/graphene samples.

In order to quantify the Raman enhancement factor of the Au NDs samples, we used the graphene area's Raman spectrum which located next to the Au NDs array area and Au nanohole as a "built-in" SERS intensity gauge. Beside the characteristic peaks of fluorescein, some additional weak peaks are also observed. These additional peaks are difficult to be assigned precisely, which may be due to the various possible interactions between substrates and fluorescein molecules, including charge transfer between metal and molecules or some damage of samples, etc. Figure 5 displays original SERS spectra which are obtained under the Au array areas and without Au array area.

Figure 6 illustrates the evaluated peaks intensity of fluorescein on different Au disc array/graphene substrates and graphene/Au nanoholes. For Au NDs samples peak intensity is evaluated using the same peak intensity which is obtained from graphene substrate as referee. For graphene/Au NHs samples, graphene/Au film is regarded as referee. The D peak of graphene is the second order scattering process involving a defect site and a phonon, and it is usually used for defect diagnosis. D band of graphene is located at 1,343 cm^{-1} and the Raman signal of fluorescein also shows one peak near D band of graphene (Fig. 4(a)). Consequently, both D band of graphene and Raman signal of fluorescein contribute the broad peak from 1,276 to 1,371 cm^{-1}. In the following evaluation, the broad peak and the peak located at 1,588 cm^{-1} corresponding to G band of graphene are ignored in order to avoid the effect of graphene. In Fig. 6, we can see the enhancement factors of seven peaks corresponding to fluorescein are different. For vibration at 1,409 cm^{-1} which belongs to C–CH bond and C–C stretch [28], the peak intensity is dramatically enhanced in comparison with other peaks. The vibration of peaks which belong to torsional motions between the xanthene ring and benzoate [32] located below 1,000 cm^{-1} exhibit less enhancement. This indicates that the LSPR really does affect the whole spectra but the enhancement efficiency for each peak is not the same. In the theory of electromagnetic models, metallic structures are always considered as efficient "hot spots" for enhancing intensity of SERS spectra and a molecule close to such structure is treated as a polarizable point dipole. Due to this hypothesis the overall enhancement is approximately equal to the product of the gain at the laser angular frequency and that at the Raman angular

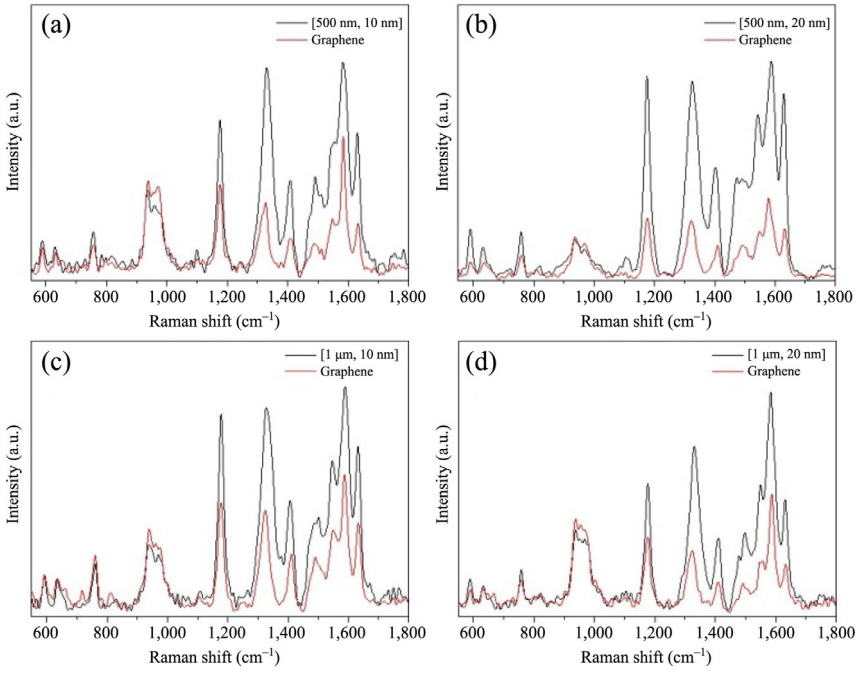

Figure 5 SERS spectra obtained from different Au discs array patterned on graphene and graphene substrate. The diameters and the thicknesses of Au NDs array are: (a) 500 nm and 10 nm, (b) 500 nm and 20 nm, (c) 1 μm and 10 nm, (d) 1 μm and 20 nm.

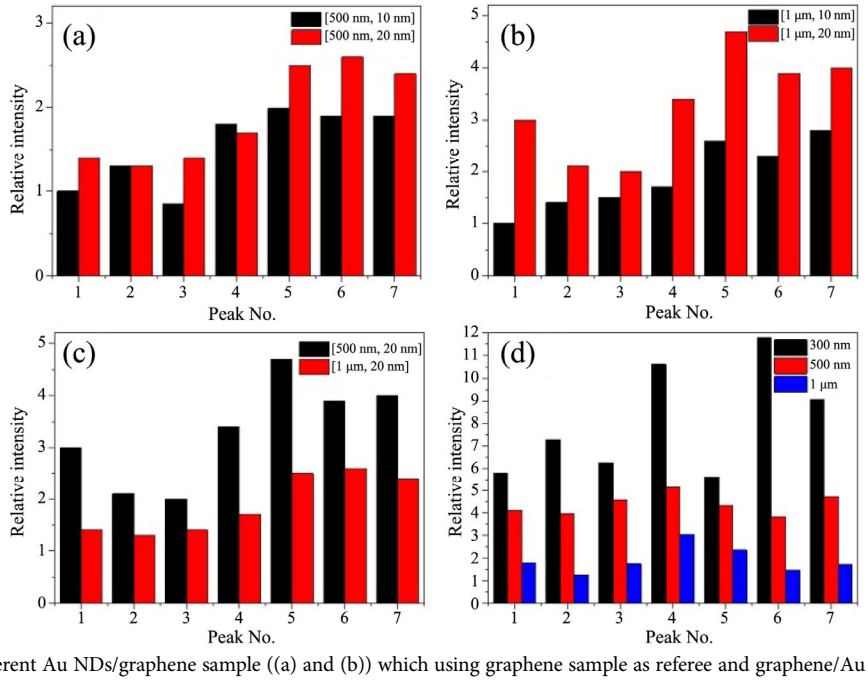

Figure 6 Peak intensity of different Au NDs/graphene sample ((a) and (b)) which using graphene sample as referee and graphene/Au NHs samples ((c) and (d)) using graphene/Au film as referee. The peak 1 to peak 7 corresponding to Raman shifts of fluorescein are located at 595, 636, 763, 1,182, 1,409, 1,549 and 1,634 cm^{-1}.

frequency [33]. According to this model, the larger enhancement can be predicted under conditions which are both frequency of the incident laser and the scattered Raman electromagnetic field approach the resonance frequency of LSPR. The theoretical analysis predicts that the maximum SERS effect occurs when the LSPR wavelength, λ_{LSPR}, is equal to half the summation of the excitation (λ_{exc}) and the Raman scattering (λ_{RS}) wavelengths; that is, $\lambda_{LSPR} = 1/2 (\lambda_{exc} + \lambda_{RS})$ [33, 34]. The absorbance spectra of Au NDs with different diameters and thickness have been plotted in Fig. S1 in the Electronic Supplementary Material (ESM). From Fig. S1 in the ESM, the absorption peaks of 500 nm diameter NDs with 10 and 20 nm thickness are 595 and 636 nm, and absorption peaks of 1 μm diameter NDs with 10 and 20 nm thickness are 616 and 673 nm. In this study, the excitation laser wavelength is fixed at 532 nm. According to the theory of LSPR theory, for the Raman peak of 1,409 cm^{-1} (which is 575 nm on wavelength scale), the calculated λ_{LSPR} is ~ 554 nm. So, the enhanced Raman intensity by Au NDs with 500 nm diameter with the λ_{LSPR} of 633 nm (which is closer to 554 nm) is larger than 1 μm NDs with the λ_{LSPR} of 673 nm. This just matches the result in Fig. 6(c). From Figs. 6(a) and 6(b) it can be observed that at the same diameter of the Au discs array the intensity of all peaks increases with increasing the thickness of Au disc. This could be due to that Au disc with large thickness can exhibit stronger electric field under light illumination. Strong electrical field interact with the molecular probe by photon–electron interaction leading to an effective amplification of the inherent weak Raman signal [35]. In Fig. 6(d), it is observed that at the same thickness of Au, the smaller diameter NHs substrates show larger SERS enhancements. This result can be affected by several factors, such as: 1) shifting of λ_{LSPR} which is caused by the changing of diameter of NDs or NHs [36]. 2) The plasmon area captured by Raman microscope is not the same. In comparison with larger diameter NDs or NHs structures, the small diameter NDs or NHs structures can contribute more plasmon region which mainly enhance the SERE signals. 3) The electromagnetic fields of the small diameter NDs or NHs are larger than big ones which is confirmed by simulation results (Fig. 7). The experimental results show that the maximal enhancement of graphene/Au NDs and graphene/Au NHs structures are 5 times larger than graphene substrate and 12 times larger than graphene/planar Au film structure, respectively.

In order to better understand the electric field enhancement of the Au NDs and Au NHs array with different diameters, the numerical simulations based on the finite-difference time-domain method simulations have been performed in Fig. 7. For Au NDs structures, the constructions were made up of hexagon gold NDs array without graphene. For the Au NHs structures, the hexagon Au NHs covered with 0.35 nm thickness graphene layer formed the simulation model. For both constructions, electric field distributions in the *XY* plane on top of structure surface have been monitored. In the simulation part, a plane light wave is launched perpendicular to the substrate with the wavelength of 532 nm. The total simulation area is 3 μm × 3 μm in the horizontal dimension and the computational domain is considered as a single unit cell. *X* axis is using anti-symmetric boundary condition and *Y* axis is using symmetric boundary condition. The structure is 50 nm thickness Au NDs array and Au NHs array. From the results of simulation, the NDs with 500 nm diameter exhibits stronger electric field than the 1 μm diameter NDs, and the 500 nm diameter Au NHs structure shows stronger electric field than NHs with 1 μm diameter. These results have good agreements with the SERS results that small diameter of NDs and NHs show larger Raman signal enhancement.

According to the simulation results, the larger electric field exists around the rim of NDs. In order to confirm the larger electric field contributes larger enhancements, the Raman intensities distributions of Au NDs with 2.5 μm diameter has been illustrated using spatially

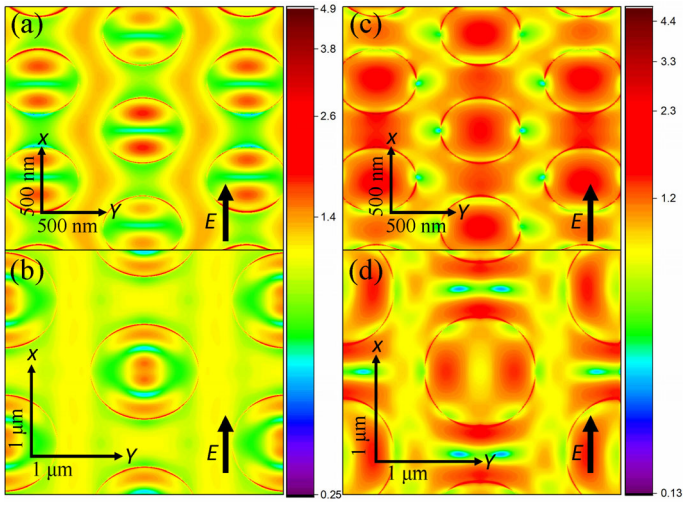

Figure 7 (a) and (b) Electric field in the plane on top of 500 nm and 1 μm Au NDs array for thickness of 50 nm. (c) and (d) Same for 500 nm and 1 μm Au NHs array for thickness of 50 nm. The colour bar value is nonlinear and the electrical value is calculated with a formula of $\log_2$(absolute electric field value) in order to enlarge the color distribution difference.

resolved Raman mapping. Figure 8 are Raman mappings of fluorescein spin-coated on 2.5 μm diameter NDs with 20 nm thickness. The scanning area is 8 μm × 8 μm and the resolution is 20 pixels × 20 pixels with a division of 400 nm. For the confocal Raman system, the Rayleigh criterion implies that the resolution cannot be physically higher than half of the spot size. The spot size which reaches the charge coupled device (CCD) can be given by the Airy disk equation, that is $S = 1.22\lambda/NA$. In which λ is the laser wavelength, *S* is the laser spot diameter, and NA is the numerical aperture of the objective. In our Raman system, the λ was 532 nm and the 50× objective (with a numerical aperture of 0.75) were applied. So, the calculated laser size was 865.4 nm. The Rayleigh criterion implies that the resolution and the maximal physical resolution cannot be physically higher than half of the spot size which was ~ 433 nm/pixel [37]. In order to cover the whole scanning area, the 400 nm/pixel parameter has been selected in this study. The color bar in Fig. 8 is nonlinear and the value of bar is calculated with formula which is $\log_2$(absolute electromagnetic field value) in order to enlarge the color distribution difference. Figure 8(a) is the Si Raman intensity distribution at 521 cm^{-1} and the background image in Fig. 8(a) is the optical image of periodic 2.5 μm NDs array. In Fig. 8(a), it is clearly observed that the Raman intensity of Au NDs covered area show less Raman intensity and the color distribution looks like "circular patterns" with the diameter of around 2.5 μm which matches the diameter of Au NDs. Figures 8(b)–8(h) are Raman distribution at peak of 595, 636, 763, 1,182, 1,409, 1,549, and 1,634 cm^{-1}, respectively. From Figs. 8(b)–8(h), it is shown that the Raman intensity at the rim of NDs is larger than the center area of NDs or substrate surface area without Au NDs deposited. Through this way, the rim of Au NDs generates larger electromagnetic field is precisely focused using Raman intensity mappings. Combing the simulation results that the rim of NDs generated larger electric field, the Raman mappings confirm the EM mechanism in SERS performances.

4 Conclusion

In conclusion, we designed a very easy, convenient and cost efficient way to generate Au NDs/graphene and graphene/Au NHs hybrid structures in this research. By combining the chemical factor of graphene and electrical magnetic field factor of plasmon structure the weak signal of molecules has been enhanced. The enhancement of molecules which spin coated on the surface of substrate exhibits

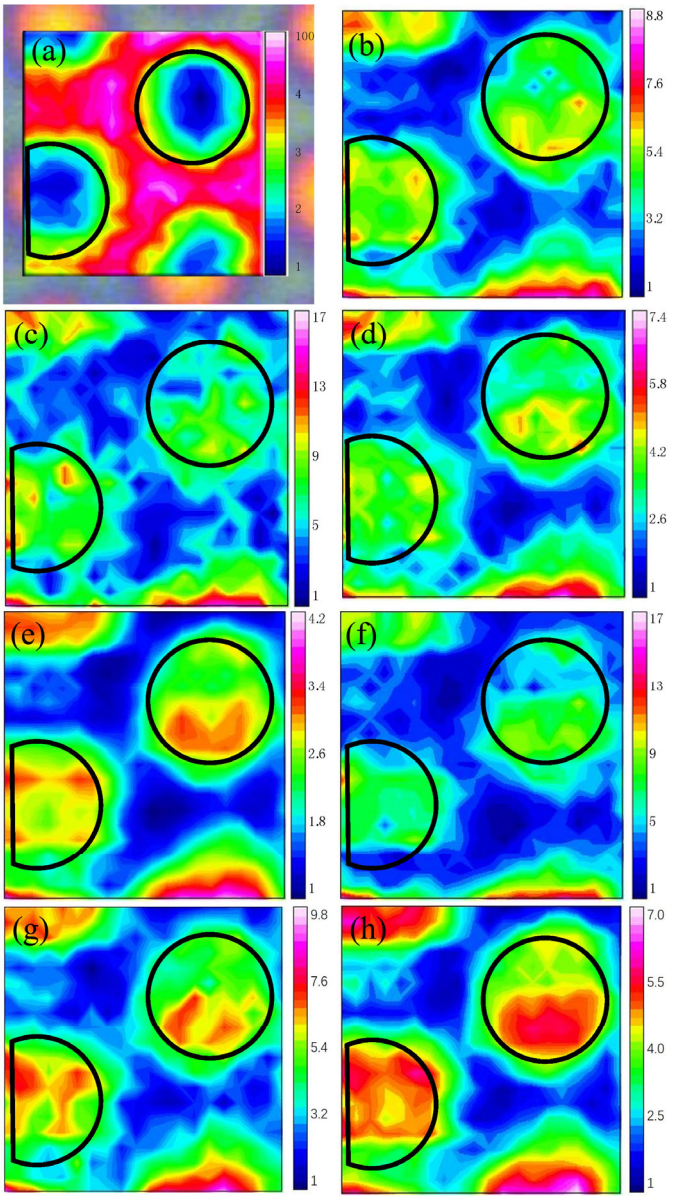

Figure 8 Raman mapping fluorescein molecules spin-coated on Au NDs/graphene substrate with 2.5 μm Au NDs diameter. (a)–(h) are integrated Raman intensities distribution of peaks located at 521, 595, 636, 763, 1,182, 1,409, 1,549, and 1,634 cm^{-1}, respectively.

systemic change through tuning the thickness and the diameter of Au NDs and Au NHs. The Raman mappings show the results that SERS enhancements at the rim of NDs are larger than that at the centre of NDs or without Au NDs region. This result has a good agreement with the simulation results that the rim of NDs generates larger electric field and confirms the EM mechanism of SERS. The fabrication method in this paper provides us a promising way to generate a highly perform platform to identify the structure of molecules by enhanced Raman signals. The Raman mapping provides a way to focus the large enhancement region. In addition, these structures, both Au NDs and Au NHs structure, provide a functional component in sensing, spectroscopy and photonic devices. In future, nanostructure fabrication with different shapes and diameters and their applications in different domains are still needed to be studied. The process of making this method as universal technique will be a long journey with practical meaning.

Acknowledgements

This work has been supported by China Scholarship Council, Chinese National Natural Science and MINISTERIO DE ECONOMÍA, INDUSTRIA Y COMPETITIVIDAD with the funding numbers of 201606180013, 51520105003 and MAT2017-89868-P, respectively.

Electronic Supplementary Material: Supplementary material (the absorbance of Au NDs with different diameters and thickness) is available in the online version of this article at https://doi.org/10.1007/s12274-019-2514-5.

References

[1] Liu, L.; Shao, M. W.; Cheng, L.; Zhuo, S. J.; Que, R. H.; Lee, S. T. Edge-enhanced Raman scattering effect from Au deposited nanoedge array. *Appl. Phys. Lett.* **2011**, *98*, 073114.
[2] Schedin, F.; Lidorikis, E.; Lombardo, A.; Kravets, V. G.; Geim, A. K.; Grigorenko, A. N.; Novoselov, K. S.; Ferrari, A. C. Surface-enhanced Raman spectroscopy of graphene. *ACS Nano* **2010**, *4*, 5617–5626.
[3] Xu, W. G.; Ling, X.; Xiao, J. Q.; Dresselhaus, M. S.; Kong, J.; Xu, H. X.; Liu, Z. F.; Zhang, J. Surface enhanced Raman spectroscopy on a flat graphene surface. *Proc. Natl. Acad. Sci. USA* **2012**, *109*, 9281–9286.
[4] Reokrungruang, P.; Chatnuntawech, I.; Dharakul, T.; Bamrungsap, S. A simple paper-based surface enhanced Raman scattering (SERS) platform and magnetic separation for cancer screening. *Sens. Actuators B: Chem.* **2019**, *285*, 462–469.
[5] Bamrungsap, S.; Treerattrakul, K. Development of SERS based biosensor for cancer screening. *Asian J. Med. Biomed.* **2018**, 28.
[6] Mosier-Boss, P. A. Review of SERS substrates for chemical sensing. *Nanomaterials* **2017**, *7*, 142.
[7] Xu, S. C.; Jiang, S. Z.; Wang, J. H.; Wei, J.; Yue, W. W.; Ma, Y. Graphene isolated Au nanoparticle arrays with high reproducibility for high-performance surface-enhanced Raman scattering. *Sens. Actuators B: Chem.* **2016**, *222*, 1175–1183.
[8] Nie, S. M.; Emory, S. R. Probing single molecules and single nanoparticles by surface-enhanced Raman scattering. *Science* **1997**, *275*, 1102–1106.
[9] Huang, X. H.; El-Sayed, I. H.; Qian, W.; El-Sayed, M. A. Cancer cell imaging and photothermal therapy in the near-infrared region by using gold nanorods. *J. Am. Chem. Soc.* **2006**, *128*, 2115–2120.
[10] Ling, X.; Xie, L. M.; Fang, Y.; Xu, H.; Zhang, H. L.; Kong, J.; Dresselhaus, M. S.; Zhang, J.; Liu, Z. F. Can graphene be used as a substrate for Raman enhancement?. *Nano Lett.* **2010**, *10*, 553–561.
[11] Otto, A.; Mrozek, I.; Grabhorn, H.; Akemann, W. Surface-enhanced Raman scattering. *J. Phys.: Condens. Matter* **1992**, *4*, 1143–1212.
[12] Balandin, A. A.; Ghosh, S.; Bao, W. Z.; Calizo, I.; Teweldebrhan, D.; Miao, F.; Lau, C. N. Superior thermal conductivity of single-layer graphene. *Nano Lett.* **2008**, *8*, 902–907.
[13] Moser, J.; Barreiro, A.; Bachtold, A. Current-induced cleaning of graphene. *Appl. Phys. Lett.* **2007**, *91*, 163513.
[14] Morozov, S. V.; Novoselov, K. S.; Katsnelson, M. I.; Schedin, F.; Elias, D. C.; Jaszczak, J. A.; Geim, A. K. Giant intrinsic carrier mobilities in graphene and its bilayer. *Phys. Rev. Lett.* **2008**, *100*, 016602.
[15] Nair, R. R.; Blake, P.; Grigorenko, A. N.; Novoselov, K. S.; Booth, T. J.; Stauber, T.; Peres, N. M. R.; Geim, A. K. Fine structure constant defines visual transparency of graphene. *Science* **2008**, *320*, 1308–1308.
[16] Ren, W.; Fang, Y. X.; Wang, E. K. A binary functional substrate for enrichment and ultrasensitive SERS spectroscopic detection of folic acid using graphene oxide/Ag nanoparticle hybrids. *ACS Nano* **2011**, *5*, 6425–6433.
[17] He, S. J.; Liu, K. K.; Su, S.; Yan, J.; Mao, X. H.; Wang, D. F.; He, Y.; Li, L. J.; Song, S. P.; Fan, C. H. Graphene-based high-efficiency surface-enhanced Raman scattering-active platform for sensitive and multiplex DNA detection. *Anal. Chem.* **2012**, *84*, 4622–4627.
[18] Chourpa, I.; Lei, F. H.; Dubois, P.; Manfait, M.; Sockalingum, G. D. Intracellular applications of analytical SERS spectroscopy and multispectral imaging. *Chem. Soc. Rev.* **2008**, *37*, 993–1000.
[19] Jones, M. R.; Osberg, K. D.; Macfarlane, R. J.; Langille, M. R.; Mirkin, C. A. Templated techniques for the synthesis and assembly of plasmonic nanostructures. *Chem. Rev.* **2011**, *111*, 3736–3827.
[20] Wang, P.; Xia, M.; Liang, O. W.; Sun, K.; Cipriano, A. F.; Schroeder, T.; Liu, H. N.; Xie, Y. H. Label-free SERS selective detection of dopamine and serotonin using graphene-Au nanopyramid heterostructure. *Anal. Chem.* **2015**, *87*, 10255–10261.

[21] Mu, C.; Zhang, J. P.; Xu, D. S. Au nanoparticle arrays with tunable particle gaps by template-assisted electroless deposition for high performance surface-enhanced Raman scattering. *Nanotechnology* **2010**, *21*, 015604.

[22] Du, Y. X.; Zhao, Y.; Qu, Y.; Chen, C. H.; Chen, C. M.; Chuang, C. H.; Zhu, Y. W. Enhanced light–matter interaction of graphene–gold nanoparticle hybrid films for high-performance SERS detection. *J. Mater. Chem. C* **2014**, *2*, 4683–4691.

[23] Xu, W. G.; Xiao, J. Q.; Chen, Y. F.; Chen, Y. B.; Ling, X.; Zhang, J. Graphene-veiled gold substrate for surface-enhanced Raman spectroscopy. *Adv. Mater.* **2013**, *25*, 928–933.

[24] Huang, Z. L.; Meng, G. W.; Huang, Q.; Yang, Y. J.; Zhu, C. H.; Tang, C. L. Improved SERS performance from Au nanopillar arrays by abridging the pillar tip spacing by Ag sputtering. *Adv. Mater.* **2010**, *22*, 4136–4139.

[25] Sivashanmugan, K.; Liao, J. D.; Liu, B. H.; Yao, C. K. Focused-ion-beam-fabricated Au nanorods coupled with Ag nanoparticles used as surface-enhanced Raman scattering-active substrate for analyzing trace melamine constituents in solution. *Anal. Chim. Acta* **2013**, *800*, 56–64.

[26] Sivashanmugan, K.; Liao, J. D.; Shao, P. L.; Liu, B. H.; Tseng, T. Y.; Chang, C. Y. Intense Raman scattering on hybrid Au/Ag nanoplatforms for the distinction of MMP-9-digested collagen type-I fiber detection. *Biosens. Bioelectron.* **2015**, *72*, 61–70.

[27] Li, X. S.; Cai, W. W.; An, J.; Kim, S.; Nah, J.; Yang, D. X.; Piner, R.; Velamakanni, A.; Jung, I.; Tutuc, E. et al. Large-area synthesis of high-quality and uniform graphene films on copper foils. *Science* **2009**, *324*, 1312–1314.

[28] Wang, L. L.; Roitberg, A.; Meuse, C.; Gaigalas, A. K. Raman and FTIR spectroscopies of fluorescein in solutions. *Spectrochim. Acta Part A: Mol. Biomol. Spectros.* **2001**, *57*, 1781–1791.

[29] Hildebrandt, P.; Stockburger, M. Surface enhanced resonance Raman study on fluorescein dyes. *J. Raman Spectrosc.* **1986**, *17*, 55–58.

[30] Ray III, K. G.; McCreery, R. L. Characterization of the surface carbonyl and hydroxyl coverage on glassy carbon electrodes using Raman spectroscopy. *J. Electroanal. Chem.* **1999**, *469*, 150–158.

[31] Xu, W. G.; Mao, N. N.; Zhang, J. Graphene: a platform for surface-enhanced Raman spectroscopy. *Small* **2013**, *9*, 1206–1224.

[32] Zhang, D. M.; Vangala, K.; Jiang, D. P.; Zou, S. G.; Pechan, T. Drop coating deposition Raman spectroscopy of fluorescein isothiocyanate labeled protein. *Appl. Spectrosc.* **2010**, *64*, 1078–1085.

[33] Yu, Q. M.; Guan, P.; Qin, D.; Golden, G.; Wallace, P. M. Inverted size-dependence of surface-enhanced Raman scattering on gold nanohole and nanodisk arrays. *Nano Lett.* **2008**, *8*, 1923–1928.

[34] Félidj, N.; Aubard, J.; Lévi, G.; Krenn, J. R.; Salerno, M.; Schider, G.; Lamprecht, B.; Leitner, A.; Aussenegg, F. R. Controlling the optical response of regular arrays of gold particles for surface-enhanced Raman scattering. *Phys. Rev. B* **2002**, *65*, 075419.

[35] Liu, D. M.; Wang, Q. K.; Hu, J. Fabrication and characterization of highly ordered Au nanocone array-patterned glass with enhanced SERS and hydrophobicity. *Appl. Surf. Sci.* **2015**, *356*, 364–369.

[36] Maurer, T.; Nicolas, R.; Lévêque, G.; Subramanian, P.; Proust, J.; Béal, J.; Schuermans, S.; Vilcot, J. P.; Herro, Z.; Kazan, M. et al. Enhancing LSPR sensitivity of Au gratings through graphene coupling to Au film. *Plasmonics* **2014**, *9*, 507–512.

[37] Foucher, F.; Guimbretière, G.; Bost, N.; Westall, F. Petrographical and mineralogical applications of Raman mapping. In *Raman Spectroscopy and Applications*. Maaz, K., Ed.; IntechOpen: London, 2017; pp 163–180.